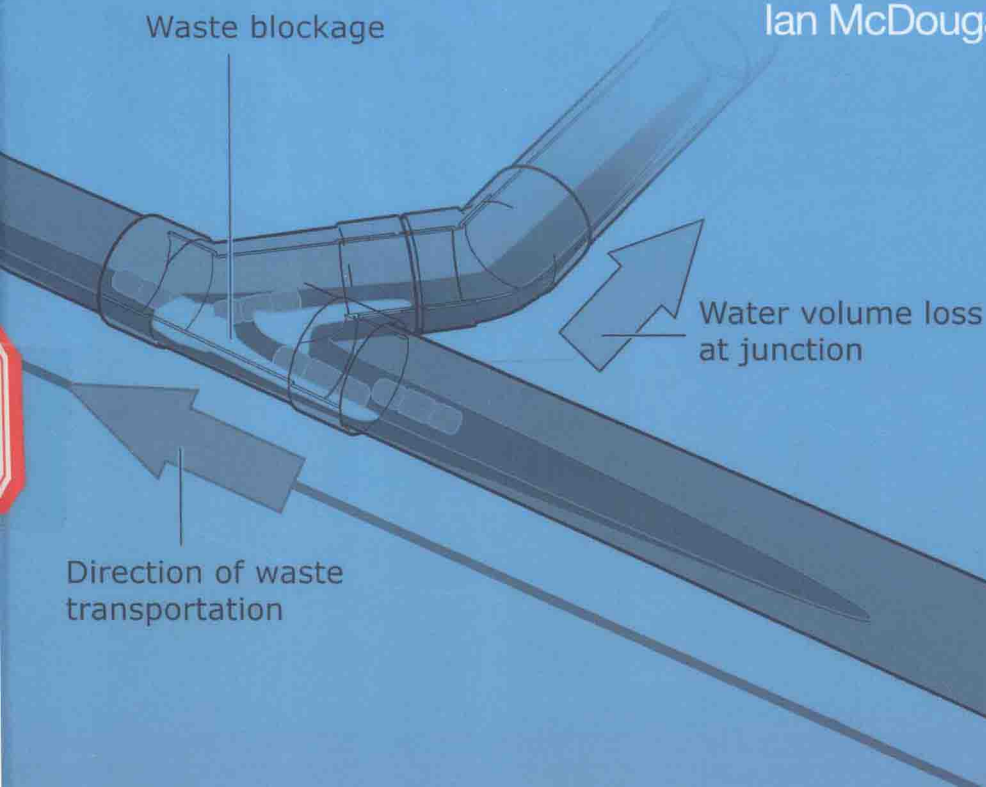


# TRANSIENT FREE SURFACE FLOWS IN BUILDING DRAINAGE SYSTEMS

John Swaffield  
with Michael Gormley,  
Grant B. Wright and  
Ian McDougall



# Transient Free Surface Flows in Building Drainage Systems

John Swaffield

with Michael Gormley, Grant Wright  
and Ian McDougall

First published 2015  
by Routledge  
2 Park Square, Milton Park, Abingdon, Oxon OX14 4RN

and by Routledge  
711 Third Avenue, New York, NY 10017

*Routledge is an imprint of the Taylor & Francis Group, an informa business*

© 2015 John Swaffield, Michael Gormley, Grant Wright and Ian McDougall

The right of John Swaffield, Michael Gormley, Grant Wright and Ian McDougall to be identified as the author of this work has been asserted in accordance with sections 77 and 78 of the Copyright, Designs and Patents Act 1988.

All rights reserved. No part of this book may be reprinted or reproduced or utilised in any form or by any electronic, mechanical, or other means, now known or hereafter invented, including photocopying and recording, or in any information storage or retrieval system, without permission in writing from the publishers.

*Trademark notice:* Product or corporate names may be trademarks or registered trademarks, and are used only for identification and explanation without intent to infringe.

*British Library Cataloguing-in-Publication Data*

A catalogue record for this book is available from the British Library

*Library of Congress Cataloging in Publication Data*

Swaffield, J. A., 1943–

Transient free surface flows in building drainage systems/John Swaffield, Michael Gormley, Grant Wright and Ian McDougall.  
pages cm

Includes bibliographical references and index

1. Hydraulic transients. 2. Drainage. 3. Sewerage. 4. Runoff. 5. Drainage pipes. I. Title.

TC171.S94 2015

696'.13—dc23

2014030683

ISBN: 978-0-415-58915-4 (hbk)

ISBN: 978-0-203-84576-9 (ebk)

Typeset in Sabon  
by Swales & Willis Ltd, Exeter, Devon, UK



Printed and bound in Great Britain by  
TJ International Ltd, Padstow, Cornwall

# Foreword

My husband John died before this book was completed, and I am grateful that members of the Drainage Research Group (DREG) at Heriot-Watt University agreed to take on the task to complete and publish it. I am indebted to them.

John was always a ‘research fellow’ at heart and wanted to leave his research and books based on his life’s work as a legacy to his new found knowledge. This has now been secured. But not only has he left his research to posterity – he has also left a team of researchers that have been inspired by his work and will take this forward in the future. I hope this book will also stimulate your interest in fluid mechanics applied to drainage systems as well.

Dr Jean Swaffield  
*February 2014*  
*Edinburgh*

# Contributors' Foreword

When John Swaffield conceived this work it was intended to be a companion book to *'Transient Airflow in Building Drainage Systems'*, which dealt with building drainage ventilation and system design from an air flow and air pressure point of view. Taken together, these two books were to encapsulate John's work in building drainage research spanning over 40 years. It is safe to say that John Swaffield was the leading academic authority on building drainage system research, and these two books were intended as his legacy to future generations of researchers.

It was with great sadness that we undertook to complete this book after John's death in 2011; however, it was felt that this book needed to be finished in order to complete the pair.

We are in little doubt that this book would have been different had John finished it himself. His unique perspective and experience in this field of study would have given the conclusions a very personal flavour. Having said that, we have tried to be as faithful to his views as much as possible, drawing on his writings as much as possible, but also on personal conversations and correspondence with him.

John is sorely missed by all who worked with him. We hope that we have done his work justice in this book and that his legacy will continue to shape the work of other researchers in this field for years to come.

Michael Gormley  
Grant Wright  
Ian McDougall  
Edinburgh  
September 2014

# Contents

<i>List of illustrations</i>	vi
<i>Foreword</i>	xix
1 Water is the new carbon	1
2 Fluid flow conditions in open channels and partially filled pipes	18
3 Solution of the governing equations of fluid flow conditions in open channels and partially filled pipes	64
4 Simulation of free surface unsteady flow in building drainage networks	129
5 Solid transport in building drainage networks	169
6 Rainwater drainage systems	217
7 Design applications	248
8 Afterword	270
<i>References</i>	274
<i>Index</i>	282

# Illustrations

1.1	Levels of relative water stress in the UK	2
1.2	Water-based climate change issues	3
1.3	Reductions in w.c. flush volume since 1880	6
1.4	Solid transport dependence on w.c. design parameters, as well as both drain and waste solid dimensions	7
1.5	Solid transport depends primarily on the volume of flush water discharged behind the solid	7
1.6	Influence of number of co-habitants on per capita water consumption	9
1.7	Projected number of households by household type, England	9
1.8	Siphonic system on Stanstead Airport	11
1.9	Siphonic system unsteady inflow/storage/outflow	11
1.10	Grey water collected v. w.c. flushing requirements	12
1.11	Q/t graphs for a 6-litre flush w.c. (in black) and a bath discharge (in grey)	13
1.12	Critical solid transport distances for multi-house installation	14
2.1	Schematic definition of free surface flow descriptors	20
2.2	The superposition of the $-c$ wave speed upon the system brings the wavefront to rest and allows the determination of the surface wave speed	22
2.3	Dependence of wave speed on flow depth, illustrated for a partially filled circular-cross section channel (100 mm diameter)	23
2.4	Dependence of attenuation on wave, flow and channel properties	24
2.5	Steady non-uniform free surface flow in a uniform conduit	25
2.6	Water and air velocity profiles in a partially filled pipe flow	27
2.7	The dependence of the Chezy coefficient on Reynolds Number and channel relative roughness	31

2.8	Values of the Chezy Coefficient based on Manning $n$ for 50% full bore flow partially filled pipe flow for a range of typical building drainage diameters	31
2.9	Increased flow capacity, 50% full bore, as the pipe slope is increased, flow predictions based on Colebrook-White with a wall roughness $k$ of 0.06 mm	32
2.10	50% full bore flow capacity comparison between Colebrook-White predictions, with a wall roughness $k = 0.06$ mm, and Chezy predictions with a Manning's $n$ of 0.009	33
2.11	Geometry of a circular-cross section drain	35
2.12	Geometrical variation of area, wetted perimeter, flow width and hydraulic mean depth for a circular cross section partially filled drain flow	35
2.13	Variation of flow mean velocity and flowrate with depth for a circular cross section	36
2.14	Variation of Normal depth with channel slope and applied flow for a 100 mm diameter drain	38
2.15	Variation of Normal and Critical depth with partially filled drain diameter and applied flow at a slope of 0.01	38
2.16	Variation of Normal and Critical depth with Manning $n$ value for a 100 mm diameter drain at 0.01 slope	39
2.17	Relationships between flowrate $Q$ , Specific Energy, $SE$ , and the boundaries of subcritical and supercritical flow defined in terms of the flow Critical depth	40
2.18	Forces acting across a hydraulic jump in steady partially filled pipe flow	44
2.19	Hydraulic jump formed upstream of a junction or flow obstruction	45
2.20	Sequent depth across a hydraulic jump formed upstream of a junction or flow obstruction in a 100 mm diameter drain at 0.01 slope with a Manning $n$ value of 0.009	46
2.21	Hydraulic jump formed downstream of a channel entry	46
2.22	Sequent depth across a hydraulic jump formed downstream of drain entry in a 100 mm diameter drain at 0.01 slope with a Manning $n$ value of 0.025	47
2.23	Sequent depth across a hydraulic jump formed downstream of drain entry in a 100 mm diameter drain at 0.0025 slope with a Manning $n$ value of 0.009	47
2.24	Gradually varied flow depth profile downstream of a vertical stack discharge to horizontal branch where the downstream flow is supercritical	48
2.25	Simpson's Rule prediction of the gradually varied flow depth profile downstream of a vertical stack	



	discharge to a horizontal branch under supercritical flow conditions	49
2.26	Gradually varied flow depth profile downstream of a vertical stack discharge to horizontal branch where the downstream flow is subcritical	49
2.27	Simpson's Rule prediction of the gradually varied flow depth profile downstream of a vertical stack discharge to horizontal branch where the downstream flow is subcritical	50
2.28	Supercritical flow exits a free discharge at its normal depth as no indication of the presence of the exit can be transmitted upstream as the wave speed is less than the flow mean velocity	50
2.29	Subcritical flow exits a free discharge at its Critical depth as information concerning the presence of the exit is transmitted upstream as the wave speed exceeds the flow mean velocity	51
2.30	Simpson's Rule predictions of the subcritical flow depth profile upstream of a free outfall at Critical depth	51
2.31	Hydraulic jumps established upstream of a multiple branch junction carrying supercritical flows	52
2.32	Simpson's Rule prediction of the depth profiles upstream and downstream of a level invert junction in a supercritical flow network	52
2.33	Hydraulic jump established upstream of a top entry branch junction carrying supercritical flows	53
2.34	Backwater profiles established upstream of a multiple branch junction carrying subcritical flows	53
2.35	Mechanism establishing annular flow below each active vertical stack to branch junction	54
2.36	Forces acting on the annular film and the basis for a terminal flow condition once the annular water film reaches a terminal velocity	55
2.37	Flowrate in a smooth vertical stack from equation 2.35 with the maximum set when the annular flow area becomes 25% of the stack cross section	57
2.38	Terminal annular velocity and development distance in a vertical stack annular water flow for a range of stack diameters	58
2.39	Development of the Steady Flow Energy Equation	60
2.40	Development of Darcy's Equation, the full bore steady flow frictional relationship in a constant cross section conduit	61
3.1	Derivation of the continuity equation for unsteady flow in a general conduit	65
3.2	Derivation of the momentum equation for unsteady flow in a general conduit	65

3.3	General free surface flow conduit properties	67
3.4	Wave speed in full bore water flow in a range of pipe materials to demonstrate impact of fluid and pipe properties	71
3.5	Method of Characteristics representation of unsteady free surface and full bore flow conditions	77
3.6	Characteristic equations available in full bore transient simulation, partially filled subcritical and supercritical conduit flows and mixed regime supercritical and subcritical flows across a hydraulic jump upstream of a junction or obstruction	79
3.7	Linear interpolation errors demonstrated within the backwater profile upstream of a subcritical free outfall	86
3.8	Time line interpolation avoids interpolation errors inherent in the linear interpolation scheme	86
3.9	Impact of TFAC > 1 on the predicted surge downstream of a sudden stoppage in a siphonic rainwater system	87
3.10	Potential for linear interpolation errors increases as the time step decreases relative to its initial value as the flow velocities within the network vary with appliance discharge	88
3.11	Cubic interpolation technique	89
3.12	Interpolation to yield MoC node depths introduces initial errors as distance increments do not match	90
3.13	Network illustrating the need to monitor branch flows and adjust the network time step to satisfy the Courant Criterion	94
3.14	Attenuation of an appliance discharge along a 20 m length of 100 mm diameter branch set at a 0.01 slope, illustrating the decrease in wave height	96
3.15	Influence of time step choice on the predicted wave attenuation along the 20 m branch drain	97
3.16	Influence of interpolation scheme on the retention of the branch drain exit Critical depth value ahead of the arrival of the appliance discharge wave	98
3.17	Influence of the chosen interpolation scheme on the rate of change of depth following the arrival of the incident appliance discharge wave	98
3.18	Time step variation based on both initial base flow, 0.1 or 1.0 litres/second, and TFAC value, 1 or 3	99
3.19	Flow depth 4 m from entry as predicted by both the LIN and NGE interpolation schemes	100
3.20	Space-time grid as a basis for a finite difference scheme, where n represents time progression and j represents the nodal number, increasing in the initial flow direction	103

3.21	Schematic representation of one version of the MacCormack method	106
3.22	Illustration of the Preismann slot to allow simulation of pressurised pipe flow	107
3.23	Typical quasi-steady bath discharge profile to a horizontal branch drain via an appliance trap seal	108
3.24	Entry to a branch drain from an appliance trap seal	109
3.25	Idealised w.c. discharge to a branch drain to represent the energy content of the inflow	110
3.26	Depth at a level invert junction	112
3.27	Depth relationships determined experimentally for two level invert junctions	113
3.28	Depth at a top entry junction	114
3.29	Flow depths upstream and downstream of an obstruction or a badly made in-line pipe junction	115
3.30	Flow depths upstream and downstream of a slope defect in a horizontal branch	116
3.31	Discharge profiles accumulate at the base of a vertical stack to establish a combined discharge to the downstream drain	117
3.32	Transition from annular to free surface horizontal flow at a stackbase	119
3.33	Flow accumulation in a vertical stack serving a number of upper floors	123
3.34	Boundary conditions necessary to simulate the movement of a hydraulic jump within branches terminating at a junction or a drain defect	124
3.35	Hydraulic jump response to an increasing approach flow and subsequent junction backflow, followed by a return to initial conditions as appliance discharge abates	125
4.1	Mechanism of wave attenuation in a partially filled channel	130
4.2	The attenuation mechanism is dependent upon the form of the applied wave	131
4.3	Schematic of DRAINET graphical user interface that allows multi-storey systems to be modelled	133
4.4	Illustrative discharge profiles to demonstrate dependence of wave attenuation on channel and appliance discharge parameters	134
4.5	Influence of pipe diameter on the attenuation in a 20 m, 100 mm diameter glass drain at a slope of 1/100 in response to a 'Plateau' format appliance discharge	135
4.6	Influence of wall roughness on the attenuation in a 20 m, 100 mm diameter drain at a slope of 1/100 in response subject to a 'Plateau' format appliance discharge	135

4.7	Influence of pipe slope on the attenuation in a 20 m, 100 mm diameter glass drain at slopes of 0.02, 0.015, 0.01 and 0.005 in response subject to a 'Plateau' format appliance discharge	136
4.8	Influence of appliance discharge profile on the attenuation in a 20 m, 100 mm diameter coated cast iron drain at a slope of 1/100 in response subject to either a 'Plateau' or 'Peak' format appliance discharge	136
4.9	Influence of leading edge rise time on the attenuation in a 20 m, 100 mm diameter coated cast iron drain at a slope of 0.01 in response subject to a 'Plateau' format appliance discharge with rise times of 0.5 and 2.0 seconds	137
4.10	Influence of baseflow on the attenuation of a 'Peak' profile format discharge in a 20 m, 100 mm diameter glass drain at a slope of 0.01 in response subject to a 'Plateau' format appliance discharge	137
4.11	Summary of attenuation dependencies	138
4.12	Peak flowrate profiles along a 20 m long, 100 mm diameter drain in response to a 'Peak' profile discharge	138
4.13	Peak flow velocity, wave speed and Froude Number profiles along a 20 m long, 100 mm diameter drain in response to a 'Peak' profile discharge	139
4.14	Peak flow velocity, depth and specific energy profiles along a 20 m long, 100 mm diameter drain in response to a 'Peak' profile discharge	139
4.15	Comparison of DRAINET predictions of wave attenuation, in terms of flowrate and wavelength, to the measurements presented by Burberry	140
4.16	Graphical representation of the predicted increasing length of the appliance discharge as it progresses along a 20 m, 100 mm diameter drain set at a slope of 1/140	141
4.17	Comparison of Wyly (1964) observation of horizontal drain flow surge capacity with DRAINET simulations (Swaffield and Galowin 1992)	141
4.18	Validation of the energy entry condition representing a w.c. discharge to a horizontal branch drain	142
4.19	Validation of the Normal and Critical depth boundary conditions representing the more tranquil discharge to a horizontal branch drain from appliances such as baths, showers or downstream of a junction or defect	143
4.20	Summed flow at the base of a two-storey vertical stack at NBS Washington, DC	144
4.21	Comparison of flow depth — the observed and predicted flow depths downstream of the vertical stack to sewer connection, NBS test installation	145
4.22	Schematic of the vertical stack and sewer connection network used to demonstrate the DRAINET simulation	

	of vertical stack entry flow to a horizontal sewer connection or multi-stack collection network	146
4.23	Comparison of the horizontal sewer connection drain entry flow profile following simultaneous and staggered w.c. discharges on the four upper floors	147
4.24	Comparison of the maximum flow depth and flowrate profiles along the 20 m, 100 mm diameter glass sewer connection branch set at 0.01 slope	148
4.25	Development and attenuation of the discharge wave along the 20 m, 100 mm diameter glass sewer connection at a 0.01 slope	148
4.26	Comparison of the horizontal sewer connection drain entry flow profile following 1.0 and 1.45 second increment staggered w.c. discharges on the four upper floors	149
4.27	Comparison of the maximum flow depth and flowrate profiles along the 20 m, 100 mm diameter glass and uncoated cast iron sewer connection branches set at 0.01 slope	150
4.28	Development and attenuation of the discharge wave along the 20 m, 100 mm diameter uncoated cast iron sewer connection at a 0.01 slope, following the 1.45 second staggered upper floor w.c. discharges	150
4.29	Comparison of the maximum flow depth and flowrate profiles along the 20 m, 100 mm diameter uncoated cast iron sewer connection branch set at 0.01 slope	151
4.30	Comparison of the entry flow profiles to the glass and uncoated cast iron sewer connections	152
4.31	Comparison of the maximum flow depth and flowrate along a 20 m sewer connection of 100 mm and 150 mm diameter at a slope of 0.01	152
4.32	Comparison of the entry flow profile generated by upper floor w.c. discharges staggered by 2 seconds in a 100 mm and a 150 mm diameter sewer connection	153
4.33	Wave attenuation along the 20 m, 150 mm, diameter uncoated cast iron sewer connection following the 2.0 second staggered set of upper floor w.c. discharges	153
4.34	Demonstration of the effect of increasing the horizontal sewer connection diameter from 100 mm to 150 mm on the full bore flow established following a series of 2 second delay upper floor w.c. discharges	154
4.35	Propagation of the full bore flow condition along the 100 mm uncoated cast iron drain in response to the inflow profile generated by upper floor w.c. discharges at a 2 second stagger	155
4.36	Initial propagation of the full bore flow condition along the 100 mm uncoated cast iron drain	155

4.37	Historic definition of flow conditions downstream of a stack to collection drain interface compared to the flow profile predicted by DRAINET for the 100 mm diameter uncoated cast iron drain	156
4.38	Level invert and top entry junction geometry utilised in the demonstrations of MoC simulations of junction-flow interaction	158
4.39	Maximum and minimum flow velocity and water depth for a 90° level invert branch junction	159
4.40	Interaction of flows from a 90° branch junction	160
4.41	Flow velocity and depth profile along the 12 m collection pipe with a 45° level invert junction at 10 m	161
4.42	Interaction of flows at a 45° level invert junction	161
4.43	Flow depths along the main collection drain (pipes 2 and 3) illustrating development of the jump position at different times for a top entry junction	162
4.44	Interaction of flows for top entry junction	163
4.45	Flow velocity and water depth at the junction for a 45° top entry junction	163
4.46	Flow velocity and water depth along the main drain line with discharge from top entry 45° junction	164
4.47	Experimental test rig used to test junction effects	165
4.48	Effect of 90° top entry junction on solid transport	166
4.49	A 45° top entry junction showing solids travelling with the predominant flow	166
4.50	Potential for higher risk of blockages from level invert junctions	167
4.51	Laboratory confirmation of potential blockage risk from level invert junction	167
5.1	Zonal description of the mechanism of solid transport in attenuating flows in a branch drain following a w.c. discharge	180
5.2	Deformable solid velocities measured in a 100 mm diameter branch drain at a range of gradients and w.c. flush volumes	182
5.3	Experimental variable slope and cross section test rig to determine the solid transport characteristics under reduced flush volume conditions	184
5.4	Branch drain cross-sectional shapes and dimensions, including the likely cross-sectional shape of the solid during transport	185
5.5	Solid velocities recorded along the circular and parabolic cross section branch drains tested at a 1/60 slope subjected to a 6 litre flush	186
5.6	Predicted peak depths and specific energy values along the various branch drains considered as an example of the effect of wave attenuation	187

5.7	Solid velocities for all branch drain cross sections, BS w.c. flush volumes and slopes, demonstrating the result of the regression analysis for one test case	189
5.8	Solid velocities for all branch drain cross sections, w.c. type, flush volumes and drain slopes, demonstrating the result of the regression analysis for all the cases considered	190
5.9	Solid deposition data compared to the predicted mean travel distance to deposition indicated by Figure 5.8	191
5.10	Branch drain slope to achieve a particular solid transport performance, indicating the steepening necessary as flush volume is decreased	192
5.11	C1 and C2 defined in terms of the solid and drain parameters as identified in equations 5.10 and 5.11	194
5.12	Dependency of deformable solid transport on a range of solid, appliance discharge and branch drain dimensionless groups	195
5.13	Experimental solid velocities for a deformable sanitary product solid discharged to a branch drain set at a range of gradients	196
5.14	Tissue deformable solid transport in a hospital interfloor void branch drain set at 1/200 slope	198
5.15	Faecal and tissue deformable solid transport in a hospital interfloor void branch drain set at 1/200 slope, illustrating the importance of tissue as a trailing solid in the continuation of faecal solid transport, previously unpublished data from Bokor (1984)	198
5.16	Stages of solid transport from inception of motion to subsequent deposition	199
5.17	Forces acting on a solid during inception of motion, subsequent motion and deposition	200
5.18	Development of the solid transport characteristic solution and identification of the solid track	202
5.19	Method of characteristics solution for unsteady free surface flows, including the representation of solid track within the x-t plane	203
5.20	Comparison of observed and predicted solid transport from rest using the boundary equations developed to describe the forces acting on the solid and the leakage flow past the solid	204
5.21	Flow depth profiles observed along the length of a cylindrical solid as the solid velocity increases from zero to the local flow velocity	204
5.22	Comparative solid transport velocity predictions for two pads differing only in base area and saturated mass	205

5.23	Solid velocity simulation derived from floating solid observations using a constant velocity decrement factor	206
5.24	Water depth difference across a solid	208
5.25	Solid velocity measurement	209
5.26	Interacting solids	210
5.27	General form of the model	212
5.28	Water depth history along pipe showing $dH_s$	213
5.29	Variation in $dH_s$ with $V_s$ when solids interact	214
5.30	Solid deposition showing stop/start motion	214
5.31	Variation in distance between solids as they travel along pipe	215
6.1	Schematic of conventional and siphonic rainwater drainage systems	218
6.2	Typical siphonic roof outlets	218
6.3	Typical gutter outlet illustrating entrained airflow exclusion baffle	218
6.4	Typical composition of a green roof	220
6.5	Typical gutter water surface profiles	221
6.6	Typical siphonic rainwater drainage system	222
6.7	Siphonic rainwater system establishment and cyclic operation	223
6.8	Impact of roof construction on runoff to gutters	228
6.9	Steady initial gutter depth profile established following imposition of a zero upstream inflow boundary condition	230
6.10	Schematic representation of the Method of Characteristics applied to full bore flow conditions	231
6.11	Gutter flow depths in a trapezoidal gutter in response to a varying rainfall intensity	233
6.12	Measured and predicted conditions for a standard gutter	234
6.13	Measured and predicted conditions for a wide gutter	235
6.14	Predicted gutter depths and overtopping rates for a 75 m section of Gutter B connected to four 110 mm diameter downpipes (roof area = 650 m <sup>2</sup> )	236
6.15	Schematic view of the Heriot-Watt siphonic roof drainage test rig	239
6.16	Measured and predicted conditions for design criteria rainfall	240
6.17	Measured and predicted conditions for a rainfall event below the design criteria	240
6.18	Measured and predicted gutter depths and system pressures from the MacCormack/MoC hybrid simulation	241
6.19	Predicted pressure surge generated by an instantaneous gutter outlet blockage	242



6.20	Predicted conditions for design criteria rainfall event, with gradually submerging system exit	243
6.21	Predicted flow rates for a siphonic system experiencing exit submergence and outlet blockage	244
6.22	Gutter depth and pipe network pressures during an extreme rainfall event at the National Archive of Scotland test site installation	245
6.23	Blockage of a siphonic roof outlet	246
7.1	Distribution of w.c. to junction distances likely in current practice	252
7.2	Demonstration three pipe network and a comparison of the transport distances achieved in 75 mm, 100 mm and 150 mm diameter pipes by a 6 litre w.c. discharge at a slope of 1/100	253
7.3	Diurnal w.c. usage patterns	254
7.4	Assumed dwelling usage pattern morning 'rush hour'	254
7.5	Layout of sanitary fittings and drainage	255
7.6	Flow rate profiles for house types 1, 2 and 3	256
7.7	Assumed pattern for a series of nine dwellings connected to common drainage	256
7.8	Simulated nine dwelling group and cumulative flow rate at end of system for 100 mm diameter pipes	257
7.9	Solid transport comparison for overall slopes of 1/60 and 1/100 illustrating the percentage of solids to clear the network and the percentage deposited in either the house to collector section or in the collector drain.	258
7.10	Simple installation to test maximum travel distance	263
7.11	Domestic installation used to test the applicability of 4 litre/2.6 litre w.c. installation	265
7.12	Importance of adjoining flows	267